Available on the CERN CDS information server **CMS PAS SUS-16-025**

CMS Physics Analysis Summary

Contact: cms-pag-conveners-susy@cern.ch 2016/08/06

Search for new physics in the compressed mass spectra scenario using events with two soft opposite-sign leptons and missing transverse momentum at 13 TeV

The CMS Collaboration

Abstract

A search for new physics in events with two low-momentum opposite-sign leptons and missing transverse momentum is presented using 12.9 fb^{-1} of data collected at 13 TeV in 2016. The observed data yields are compatible with the predictions for standard model processes. The results are interpreted in the context of supersymmetry with compressed mass spectra, described in the form of simplified models. In the first model the lightest chargino ($\tilde{\chi}_1^{\pm}$) and the second-lightest neutralino ($\tilde{\chi}_2^0$) are pair produced and degenerate in mass, and decay to the lightest neutralino and a virtual W and Z boson, respectively. At 95% confidence level, $\tilde{\chi}_1^{\pm}/\tilde{\chi}_2^0$ masses are excluded up to 175 GeV for a mass difference of 7.5 GeV with respect to the lightest neutralino. Previously such a scenario had only been constrained by LEP experiments. The results are also interpreted in a simplified model of top squark pair production for the case that the mass difference between the top squark and the lightest neutralino is below the mass of the W boson.

1 Introduction

Numerous searches for new physics involving dark matter particles at hadron colliders rely on signatures that include large missing transverse momentum, $E_{\mathrm{T}}^{\mathrm{miss}}$, along with leptons and/or hadronic jets of high transverse momentum, p_{T}. This search requires $E_{\mathrm{T}}^{\mathrm{miss}}$ and two low momentum leptons of opposite charge, which dramatically reduces the standard model (SM) background compared to analyses with one or zero leptons. A particle mass spectrum is referred to as "compressed" when some of its particles are nearly degenerate in mass. Such spectra can arise in natural supersymmetry (SUSY): it has been pointed out by several authors, including [1–6], that naturalness imposes constraints on the masses of higgsinos, top squarks ($\tilde{\mathrm{t}}$) and gluinos. As pointed out in [7–9], light higgsinos would likely have a compressed mass spectrum, potentially leading to signatures with soft leptons and moderate or significant $E_{\mathrm{T}}^{\mathrm{miss}}$. Natural SUSY is generally considered to require at least one colored particle to have relatively low mass below ~ 1 TeV. It is commonly assumed that this particle would be a third-generation squark, e.g. $\widetilde{\mathrm{t}}$. More recently, however, this hypothesis of a light $\widetilde{\mathrm{t}}$ has been disputed as arising from an oversimplified calculation [8]. Nevertheless, even with these simplifications, higgsinos remain light and present a complementary window to accessing natural SUSY. Thus far, the most sensitive searches in this scenario have been carried out by experiments at LEP [10–12].
The current analysis has been conceived to search for signs of gauginos (also referred to as "electroweakinos" in what follows) in a compressed mass spectrum. The analysis is also applicable for the case where a light $\widetilde{\mathrm{t}}$ and the lightest SUSY particle (LSP) are nearly degenerate in mass and the $\widetilde{\mathrm{t}}$ decays to four fermions. The nearly mass degenerate region of the $\widetilde{\mathrm{t}}$ and the LSP is the so-called "co-annihilation region", which allows for dark matter to be provided solely by the LSP [13].
The strategy of the current analysis is similar to the one in [14], which was carried out at a center-of-mass energy of 8 TeV. The main difference lies in the deployment of a new trigger selection, which increases the sensitivity of the search. The selection in [14] has also been extended to be optimal for electroweakinos with a compressed mass spectrum. As in the 8 TeV analysis, events containing a b-tagged jet are rejected, in order to reduce the very significant background from $\mathrm{t\bar{t}}$ production and decays. At least one jet is required in the final state, which in the case of the signal must arise from QCD initial state radiation (ISR) and which provides the final-state particles with a boost in the transverse plane and thus the potential for a moderate or large $E_{\mathrm{T}}^{\mathrm{miss}}$. Contrary to the 8 TeV analysis, the search is inclusive in the number of jets, i.e. there is no upper limit on the number of jets in the event.

2 Data and simulated samples

The data used in this search correspond to 12.9 fb^{-1} of pp collisions at a centre-of-mass energy of 13 TeV, recorded in 2016 with the CMS detector. The data are selected with two triggers: an inclusive $E_{\mathrm{T}}^{\mathrm{miss}}$ trigger, where the $E_{\mathrm{T}}^{\mathrm{miss}}$ threshold varied from an initial value of 90 GeV to larger values as the instantaneous luminosity of the LHC increased. The second trigger was introduced after the first technical stop of LHC in 2016, with a lower threshold of $E_{\mathrm{T}}^{\mathrm{miss}} > 50$ GeV and the requirement of two muons with $p_{\mathrm{T}} > 3$ GeV. The sample with inclusive $E_{\mathrm{T}}^{\mathrm{miss}}$ triggers corresponds to an integrated luminosity of 12.9 fb^{-1}, whereas the sample recorded with the dimuon + $E_{\mathrm{T}}^{\mathrm{miss}}$ trigger corresponds to 10.1 fb^{-1}.
Simulated samples of the signal, $\mathrm{t\bar{t}}$, W+jets, and Z+jets processes are generated at leading-order (LO) with the MADGRAPH5 [15] event generator, using the NNPDF3.0LO [16] parton distribution functions (PDFs). For di-boson, single top quark and rare processes, the next-to-leading order generators MADGRAPH5_aMC@NLO [17] and POWHEGv1.0 [18–22] are used with

the NNPDF3.0NLO [16] PDFs. Showering and hadronization is carried out by the PYTHIA 8.2 package [23], while a detailed simulation of the CMS detector is based on the GEANT4 [24] package. A fast detector simulation [25] is used to produce large signal samples corresponding to different sparticle masses, the so-called "signal scans".
Neutralino-chargino ($\widetilde{\chi}_2^0$-$\widetilde{\chi}_1^\pm$) pair production is considered for the electroweakino scan. The $\widetilde{\chi}_2^0$ and $\widetilde{\chi}_1^\pm$ are assumed to decay to the LSP via virtual Z* and W* bosons. For the virtual Z* boson the SM branching ratios for decays to the different fermions as a function of the maximal fermion pair mass M(ff) are applied. The maximal M(ff) is the mass difference between $\widetilde{\chi}_2^0$ and $\widetilde{\chi}_1^0$. The simulation of the $\widetilde{\chi}_2^0$ decay takes the Breit-Wigner shape of the Z boson into account. The production cross sections used correspond to those for pure Wino production.
The second scan simulates $\widetilde{\mathrm{t}}$-pair production, where each $\widetilde{\mathrm{t}}$ decays to $\ell\nu\mathrm{b}\widetilde{\chi}_1^0$. The mass difference between $\widetilde{\mathrm{t}}$ and $\widetilde{\chi}_1^0$ is less than 90 GeV. The branching ratios to leptons are set equal to those for top quark decays and the $\widetilde{\mathrm{t}}$ decay length is set to zero[1]. Figure 1 illustrates the signal models considered.

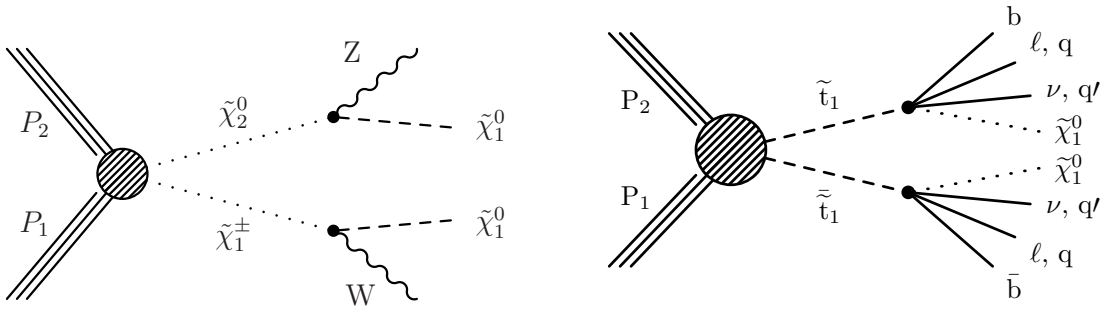

Figure 1: Left: electroweakino pair production. Right: $\widetilde{\mathrm{t}}$ four-body decay. The model used to interpret the results represents a simplified version of the four body decay in which the top quark decay width is neglected.

3 Object reconstruction

The physics objects used in the analysis are reconstructed and selected using CMS standard algorithms and requirements. The effects of the contributions from additional proton-proton interactions within the same or neighboring bunch crossings (pileup) are mitigated using primary vertex selection and other methods described in the following.

Primary vertices are identified using tracks clustered with the deterministic annealing algorithm. The reconstructed primary vertex is chosen as the vertex with the largest quadratic sum of the p_T of its constituent tracks. Additionally, this vertex needs to be within 24 cm from the center of the detector in the z direction and within 2 cm on the plane transverse to the beam line.

Leptons are reconstructed using the CMS particle-flow (PF) algorithm [27] and their p_T and pseudorapidity (η) are required to be inside the trigger acceptance and within the boundaries of the inner tracker. The leading muon (electron) is thus required to satisfy $p_\mathrm{T} > 5, |\eta| < 2.4$ ($|\eta| < 2.5$). An upper cut of $p_\mathrm{T} < 30\,\mathrm{GeV}$ on the leading lepton is also applied; this limit is identified as the p_T value below which the current analysis is more sensitive in excluding the

[1] In full SUSY models, the suppression of the four body decay at small ΔM ($< 30\,\mathrm{GeV}$) leads to displaced vertices [26]. This effect is not taken into account in the current search: all particles are assumed to decay promptly

benchmarks in the compressed regions, compared to other analyses in CMS. In some of the final categories of this analysis, the lower p_T threshold of the subleading muon is set to 3.5 GeV in order to further increase the sensitivity to the compressed regime. Muons are required to pass the soft muon identification [28] and to be isolated within a cone in $\eta - \phi$ space of radius $\Delta R = \sqrt{\Delta\eta^2 + \Delta\phi^2} < 0.3$: the sum of the transverse momenta within the cone are required to be less than 5 GeV, and also to be less than 0.5 times the p_T of the muon. Contamination from pile-up within the isolation cone is subtracted using techniques that utilise charged deposits inside the cone itself [28].
Identification of electrons coming from prompt decays is performed using a multivariate discriminant based on shower shape and track quality variables. The loose working point (WP) employed by the $H \to ZZ \to 4\ell$ analysis [29] is used for $p_T < 10$ GeV, and a tighter one for $p_T > 10$ GeV. The same isolation criteria as for the muons are applied.
To suppress non-prompt leptons, cuts on the impact parameter with respect to the primary vertex, both in the transverse plane, d_{xy}, and along the z (beam) direction, d_z, are applied: leptons are required to have $|d_{xy}| < 0.01$ cm and $|d_z| < 0.01$ cm.

Jets are clustered from the particles reconstructed by the PF algorithm [27]. In the jet clustering procedure, charged PF particles not associated with the primary vertex are excluded. The anti-k_T jet clustering algorithm [30] is used with a distance parameter R = 0.4. The jet energy scale (JES) is measured in data using dijet and photon plus jets events, and a correction is applied to both data and simulated samples. Jets are selected to satisfy $p_T > 25$ GeV and $|\eta| < 2.4$. In the following, the transverse hadronic energy, H_T, is defined as the scalar sum of the jet transverse momenta having $p_T > 25$ GeV.

Identification of b jets is done via the Combined Secondary Vertex (CSV) tagger [31]. In this analysis the *Loose* WP is used, which has a nominal efficiency of about 80% (for a udsg-mistag efficiency of 10%). Since the analysis focuses on final states with soft leptons, b-jets events tagged by the CSV Loose WP with $p_T > 25$ GeV are vetoed. This allows for potential soft b-tagged jets coming from e.g. the compressed $\tilde{t}$-LSP scenario.

Missing transverse energy in the event (E_T^{miss}) is based on PF reconstructed quantities. Various event filters are applied to remove the detector- and beam-related noise.

4 Event selection

The analysis requires two opposite-sign (OS) leptons ($N_\ell = 2$), of either the same flavor (ee, $\mu\mu$) or different flavor (eμ), and moderate missing transverse energy in the final state, together with the presence of at least one jet in the event. Leptons and the hadronic content of the event, jets and E_T^{miss} are identified according to the criteria listed in Section 3.
A complete set of requirements that define the signal region (SR) is listed in Table 1. The main backgrounds arise from events in which one of the leptons is not prompt (mainly in W+jets events), events from fully leptonic $t\bar{t}$ decays and Drell-Yan (DY) processes with subsequent decays of the γ/Z^* to $\ell\ell\nu\nu\nu$ via τ leptons. A small background is due to relatively rare diboson processes like WW (VV) and t+W (tW) production. The event selection in Table 1 includes a number of requirements that are designed to reduce these backgrounds:

- $0.6 < E_T^{miss}/H_T < 1.4$: H_T is the sum of all jet momenta. This criterion is effective in rejecting QCD events while it is efficient for events with ISR, as in the case of the signal. The upper bound on the ratio E_T^{miss}/H_T is determined from a study of a control region at low E_T^{miss} and dimuon mass around the J/Ψ. The cut rejects such events while leaving the signal intact.

- b-jet event veto: Requiring events where no jet is tagged as originating from a b quark reduces significantly the $t\bar{t}$ background where the b jets are coming from the decay of the top quarks. The requirement is applied to all jets with $p_T > 25$ GeV and using b-tag selection criteria described in Section 3.
- $M_{\tau\tau} < 0$ or $M_{\tau\tau} > 160$ GeV: this requirement is designed to reject the large background from $Z \to \tau\tau$ events, with the τ leptons subsequently decaying leptonically. The quantity $M_{\tau\tau}$ is computed as follows: since the τ leptons from Z boson decays have high momenta, $p_T(\tau) \gg m_\tau$, the direction of the final lepton, i.e. the observed electron or muon, is approximately the same as that of the parent τ (i.e. $\Delta R(\ell, \tau) \sim 0$). The magnitude of the lepton vectors are then scaled so that the lepton pair balances the hadronic recoil. For $Z \to \tau\tau$ events, this leads to a fairly good approximation of the original τ momenta. The invariant mass of the two τ leptons, $M_{\tau\tau}$, is estimated as the invariant mass of the two scaled leptons. In some events, the estimate of the τ momentum leads to a negative value, i.e. opposite to the direction of the lepton. In these cases the invariant mass $M_{\tau\tau}$ is set to be negative.
- $M_T(\ell_i, E_T^{miss}) < 70$ GeV, i=1,2: for the signal, the leading lepton is typically aligned with the boost direction of the LSP ($\Delta\phi(\ell, E_T^{miss}) \sim 0$). This cut is particularly effective in further suppressing the $t\bar{t}$ background. It is not, however, particularly effective in the discrimination of the $\tilde{t}$ signal and thus it is not used in the $\tilde{t}$-like signal region.
- J/Ψ and Υ veto: to suppress potential background contributions from J/Ψ, γ^* and Υ decays, the di-lepton invariant mass, $M(\ell\ell)$, is required to satisfy $M(\ell\ell) > 4$ GeV and we veto events with $9 < M(\ell\ell) < 10.5$ GeV.
- $E_T^{miss} > 125$ GeV: to ensure high trigger efficiency for the kinematic region used in the analysis, both the E_T^{miss} and the muon corrected $E_T^{miss}{}_{corr}$, which is computed from the vectorial sum of the E_T^{miss} and the p_T of the muons selected in the events, are required to be larger than 125 GeV.
- Trigger acceptance: at the trigger level the lepton pair is required to have a small boost of $p_T > 3$ GeV and to have an upper bound on the dimuon invariant mass, $M(\ell\ell) < 60$ GeV, in order to limit the trigger rate. This imposes an upper cut of 50 GeV on the invariant mass of the leptons selected offline and a lower cut on the dilepton transverse momentum $p_T(\ell\ell) > 3$ GeV.
- $H_T > 100$ GeV: this requirement suppresses backgrounds with low hadronic activity in the event.

4.1 Signal region categorization

The analysis targets two categories of signal events with different characteristics. The first category corresponds to the presence in the decay chain of a Z* that is constrained in mass, e.g. like in the decays of $\tilde{\chi}_2^0$ to $\tilde{\chi}_1^0$. This leads to same-flavor opposite-sign leptons with invariant mass that has a maximum value that corresponds to the mass difference between the two gauginos. To increase the analysis sensitivity to this scenario, the search region is divided in four regions of $M(\ell\ell)$: 4-10, 10-20, 20-30, and 30-50 GeV.
The second category corresponds to the two leptons stemming from two different particles, as in the decays of two top squarks, or in two cascades like $\tilde{\chi}_1^\pm$ to $W^*\tilde{\chi}_1^0$. In these cases, the leptons are not required to have the same flavor. For this scenario events are categorised according to the p_T of the leading lepton in four regions, namely 5-12, 12-20, and 20-30 GeV. The second lepton p_T threshold is reduced to 3.5 GeV for muons in the high E_T^{miss} region to gain sensitivity in the $\tilde{t}$-like signal categorization.

Table 1: Selection requirements for the signal regions. The subleading lepton p_{T} threshold is reduced to 3.5 GeV for muons in the high $E_{\mathrm{T}}^{\mathrm{miss}}$ $\widetilde{\mathrm{t}}$-like signal region. Iso_{rel} and Iso_{abs} are relative and absolue isolation.

Variable	SR selection criteria
N_ℓ	$= 2$ (ee,$\mu\mu$, eμ)
Q(ℓ_1)Q(ℓ_2)	-1
$p_{\mathrm{T}}(\ell_1)$, $p_{\mathrm{T}}(\ell_2)$	$[5, 30]$ GeV
$p_{\mathrm{T}}(\mu_2)$ for high $E_{\mathrm{T}}^{\mathrm{miss}}$ $\widetilde{\mathrm{t}}$-like SR	$[3.5, 30]$ GeV
$\lvert\eta_\mu\rvert$	< 2.4
$\lvert\eta_{\mathrm{e}}\rvert$	< 2.5
$d_z(\ell_{1,2})$ & $d_{xy}(\ell_{1,2})$	< 0.01 cm
$Iso_{\mathrm{rel}}(\ell_{1,2})$ & $Iso_{\mathrm{abs}}(\ell_{1,2})$	< 0.5 & < 5 GeV
$p_{\mathrm{T}}(jet1)$	> 25 GeV
$\lvert\eta\rvert(jet1)$	< 2.4
N_b (>25 GeV, CSVL)	$= 0$
$M(\ell\ell)$	< 50 GeV
$p_{\mathrm{T}}(\ell\ell)$	> 3 GeV
$E_{\mathrm{T}}^{\mathrm{miss}}$	> 125 GeV
$E_{\mathrm{T}}^{\mathrm{miss}}$ (muon subtracted)	> 125 GeV
$E_{\mathrm{T}}^{\mathrm{miss}}$ / H_{T}	$[0.6, 1.4]$
H_{T}	> 100 GeV
$M(\ell\ell)$	> 4 GeV
$M(\ell\ell)$	veto$[9, 10.5]$ GeV
$M_{\tau\tau}$	veto$[0, 160]$ GeV
$M_{\mathrm{T}}(\ell_x, E_{\mathrm{T}}^{\mathrm{miss}}), x = 1, 2$	< 70 GeV (for electroweakino selection only)

To fully exploit the potential of the dimuon plus $E_{\mathrm{T}}^{\mathrm{miss}}$ trigger introduced in 2016, an additional separation between the high $E_{\mathrm{T}}^{\mathrm{miss}}$ and low $E_{\mathrm{T}}^{\mathrm{miss}}$ regions is added by splitting around the $E_{\mathrm{T}}^{\mathrm{miss}}$ value of 200 GeV. Since the low $E_{\mathrm{T}}^{\mathrm{miss}}$ region contains events accessible only via the new trigger, only $\mu^+\mu^-$ pairs are considered. Conversely, in the high $E_{\mathrm{T}}^{\mathrm{miss}}$ region both electron and muon flavors are considered. The electroweakino-like SR is populated by $\mathrm{e}^+\mathrm{e}^-$ and $\mu^+\mu^-$ pairs, while for the $\widetilde{\mathrm{t}}$-like SR also eμ pairs are allowed.

5 Background estimation

Backgrounds with two prompt leptons are estimated using control regions that are identified to be similar in phase space to the signal regions, yet remain relatively signal free. Different control regions are employed for each physics process that contributes significantly in the signal region, namely the $\mathrm{t\bar{t}}$ dilepton background, the DY+jets background and the diboson background.

The background in the signal region (SR) is estimated independently for each physics process, using the number of events observed in the data in the corresponding control region (CR) and a transfer factor which describes the expected ratio of events in the SR and in the CR region for each physics process. The transfer factor for a specific physics process, F_{process}, is determined from Monte Carlo (MC) simulation of the process as the ratio

$$F_{\text{process}} = \frac{N^{SR}_{\text{MC process}}}{N^{CR}_{\text{MC process}}}$$

If the corresponding CR in the data consisted solely of events from the physics process in question, e.g. DY+jets events, then the background estimate in the SR would be given as

$$N^{SR}_{\text{process}} = N^{CR}_{\text{data}} F_{\text{process}}$$

Effectively, this estimate assumes that the simulation describes well the kinematic dependence of the physics process, and normalizes the expected yield from the physics process in question to the one observed in the corresponding CR in the data. Deviations from this assumption are accounted for as systematic uncertainties in the value of the transfer factor.

The CR contains contributions from other physics processes that need to be subtracted from N^{CR}_{data}. These contributions, $N^{SR}_{\text{MC other}}$, are estimated using MC simulation, and the final estimate of the background from a specific physics process in the SR is given by

$$N^{SR}_{\text{process}} = \left(N^{CR}_{\text{data}} - N^{SR}_{\text{MC other}} \right) F_{\text{process}}$$

Systematic uncertainties on the value of F_{process} are included in determining the full uncertainty on N^{SR}_{process}. The total background in the SR is given as the sum of the backgrounds expected from each process using this method.

The different CRs are binned in $E_{\mathrm{T}}^{\mathrm{miss}}$, but not in $M(\ell\ell)$ or lepton p_{T}. A summary of all the CRs for prompt leptons is given in Table 2. For the diboson background, a validation region enriched in WW is added. This region is used to establish how well the simulation agrees with data in order to validate the uncertainty assigned to the diboson (VV) simulation.

Table 2: Summary of selection of control regions and the WW validation region (VR).

CR DY+jets	CR $\bar{\text{tt}}$	VR VV
no upper cut on p_{T} (ℓ) $Iso_{\text{rel}} < 0.1$ as OR to SR isolation		
$0 < M_{\tau\tau} < 160$ GeV Max(d_{xy},d_z) < 0.03 cm		
p_{T} (ℓ1) > 20 GeV OR Min(d_{xy},d_z) > 0.01 cm M_{T} as for EWKino SR	 M_{T} as for stop SR	p_{T} (ℓ1) > 20 GeV $\lvert$ M($\mu\mu$ or ee) - M(Z)$\rvert > 10$ GeV $M_{\text{T}} > 90$ GeV
	at least one b-tagged jet with $p_{\text{T}} > 40$ GeV	

5.1 The DY+jets control region

The main difference between the control region for the DY+jets background and the signal region of the analysis lies in the requirement imposed on the $M_{\tau\tau}$ variable: the CR consists of the events that are vetoed in the signal region selection, i.e. those events with $M_{\tau\tau}$ in the range 0-160 GeV. To further increase the efficiency for leptons from τ decays, the impact parameter variable cuts are relaxed to 300 μm. Finally, the upper bound of 30 GeV on the lepton p_{T} is removed. The region with lepton $p_{\text{T}} < 20$ GeV and $\min(d_{xy}, d_{xy}) < 0.01$ is removed to reduce the effect of potential signal contamination.

Figure 2 shows the $M(\ell\ell)$ distribution of the control sample. The trigger, lepton identification and b-tagging efficiencies are corrected in the simulation via the application of scale factors measured in dedicated data control samples. Overall good agreement is observed. Moreover, the shapes of the distributions of the variables used to bin the signal regions, $M(\ell\ell)$ and the leading lepton p_{T}, are well described. The event yields estimated from simulation and the observed event yields are listed in Table 3. The residual physics processes other than DY+jets production are subtracted from the data using the simulation before the data-to-simulation ratio is evaluated for the estimate.

Table 3: Data and simulation yields for the DY and $\bar{\text{tt}}$ control regions corresponding to a integrated luminosity of 12.9 fb^{-1} (high $E_{\text{T}}^{\text{miss}}$ region) and 10.1 fb^{-1} (low $E_{\text{T}}^{\text{miss}}$ region). Uncertainties are statistical.

	DY		$\bar{\text{tt}}$	
$E_{\text{T}}^{\text{miss}}$	125-200 GeV	> 200 GeV	125-200 GeV	> 200 GeV
CR process (DY or $\bar{\text{tt}}$)	68.6 ± 6.3	78.3 ± 2.3	346.0 ± 6.4	230.3 ± 6.5
All SM processes	75.2 ± 6.4	88.5 ± 2.7	391.6 ± 7.5	321.0 ± 8.4
Data	81	106	342	285

5.2 The $\bar{\text{tt}}$ (2l) control region

To obtain a sample enriched in $\bar{\text{tt}}$ events, one or two jets are required to be identified as originating from b quarks (b-tagged). To reduce potential signal contamination, the leading b-tagged jet is required to satisfy $p_{\text{T}} > 40$ GeV. To increase the number of events in the CR, while still avoiding potentially large signal contamination, the upper bound on the lepton p_{T} is also removed. Figure 2 shows the $M(\ell\ell)$ distribution of the control sample for both $E_{\text{T}}^{\text{miss}}$ bins. The trigger, lepton identification and b-tagging efficiencies are corrected in the simulation via the application of scale factors measured in dedicated data control samples. The event yields estimated from simulation and the observed event yields are shown in Table 3. The amount of simulated residual processes not classified as $\bar{\text{tt}}$ background are subtracted from data before the data to simulation ratio is evaluated for the $\bar{\text{tt}}$ prediction in the signal regions.

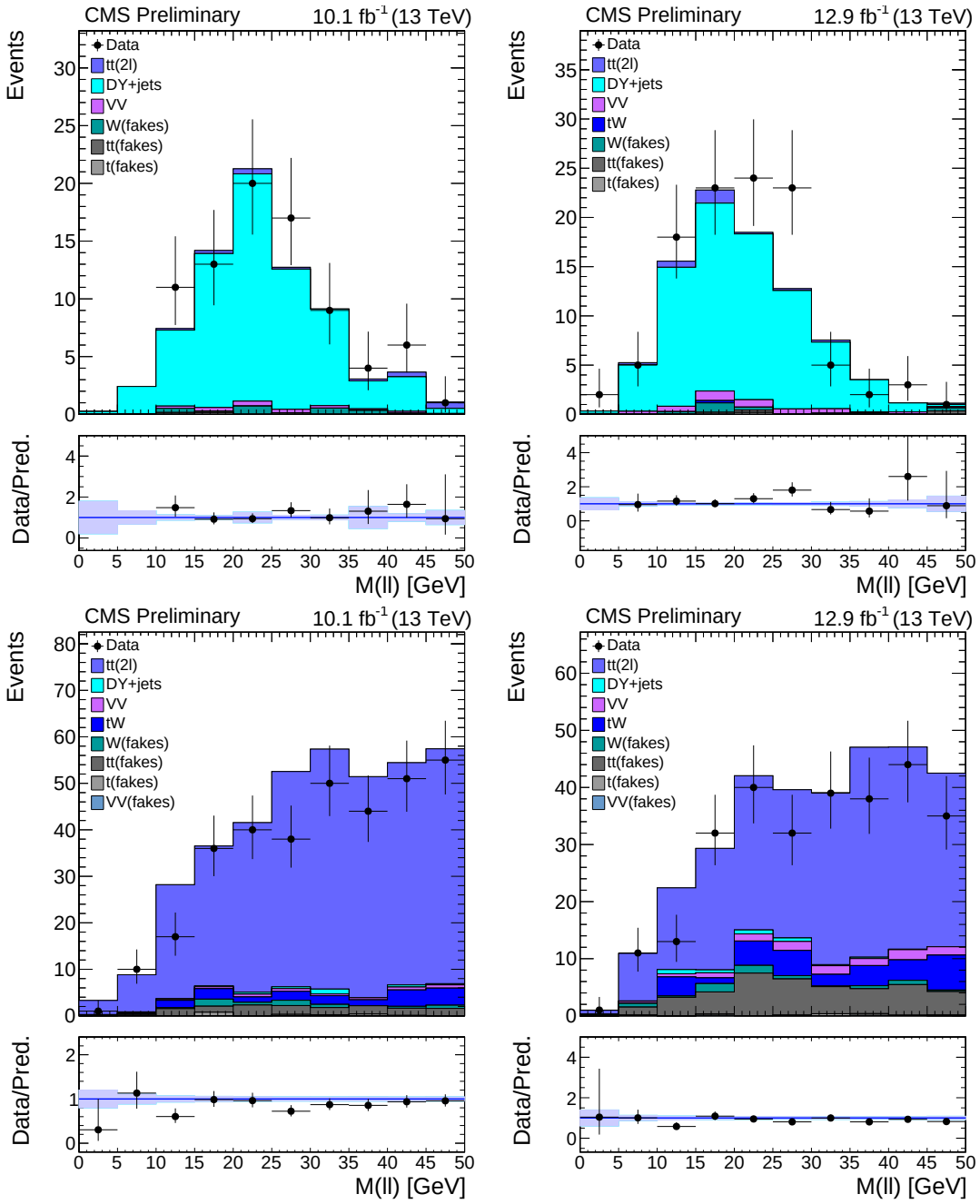

Figure 2: $M(\ell\ell)$ distributions for DY+jets (top) and $t\bar{t}$ (bottom) control regions. Left: control regions with low E_T^{miss}. Right: control regions with high E_T^{miss}. The bands in data/prediction ratio reflect the statistical uncertainty on the simulation.

5.3 Non-prompt background

The background from non-prompt leptons is evaluated using a "tight-to-loose" method. The "non-prompt" background is also sometimes referred to as "fakes" background. Events where at least one lepton fails the tight identification and isolation criteria but passes a looser selection ("application region") are weighted by a transfer factor based on the probabilities that non-prompt and prompt leptons, passing the loose requirements, also satisfy the tight ones.

The probability for non-prompt leptons ("fake-rate") is measured as a function of the lepton p_T and η using a data sample enriched in QCD multijet events ("measurement region"). The method has been used in several multilepton searches in CMS and is described in more detail in [32]. The measurement region is defined by the presence of exactly one loose lepton and a jet with $p_T > 30\,\text{GeV}$, separated from the lepton by $\Delta R > 0.7$. For muons, events are selected by prescaled single-lepton triggers with no isolation requirements. For electrons, a mixture of prescaled jet triggers is used. An important challenge comes from the existence of prompt leptons in the the measurement region, mostly due to W and Z production in association with jets. This electroweak contamination is subtracted using three alternative procedures that yield consistent results.

The probability for prompt leptons is taken from simulation and corrected with a data-to-simulation scale factor extracted from $Z \to \ell\ell$ events.

The fake-rate measured in QCD events has to be applied to a sample dominated by W + jets and $t\bar{t}$ events. The latter can have a different composition in terms of flavour of the jets that give rise to the non-prompt leptons, along with other kinematic differences that potentially affect the fake-rate. These effects are studied first of all by comparing the fake-rate in the simulation of these processes; consistent results across the phase space probed by this analysis are found. A closure test is then performed by applying the fake-rate measured in the QCD simulated sample to a sample of W + jets events. The yield of events passing the tight identification criteria is compared with the prediction obtained by applying the fake-rate in the application region. The method closes at a level of 30% or better; this value is used as a systematic uncertainty on the reducible background prediction when performing the signal extraction.

6 Systematic uncertainty on the background prediction

The systematic uncertainties on the background predictions are reported and discussed below. The given uncertainties are relative to the total number of events predicted.

- Statistical uncertainty from data yields in control and application regions:
  The statistical uncertainty is dominated by the small number of events in the "tight-to-loose" application region. It typically dominates over the other uncertainties of the prediction especially for signal regions with small event yields. It ranges from 20% to 80% depending strongly on the amount of yields in the predicted region.
- Statistical uncertainty from simulation:
  As the ratios of expected yields in control and signal regions are taken from simulation, the statistical uncertainty on the simulated events affects the prediction. It typically ranges from 10-20% for $t\bar{t}$ and DY+jets events.
- $t\bar{t}$ transfer factor uncertainties:
  The spin correlation of the top quarks has been varied by 20%, following the measurement of CMS and ATLAS [33, 34] and also from the comparison with different generators (MADGRAPH versus POWHEG). Helicity amplitudes of the W boson are

varied by 5%. A top p_T modeling uncertainty was derived from data to simulation comparisons and is applied. The combined effect of the set of $t\bar{t}$ modeling uncertainties on the total number of predicted background is typically in the order of few percent.

- DY+jets transfer factor uncertainties:
  The closure test for the DY+jets control sample in data leads to 15% uncertainty for the DY+jets predictions. The test captures the uncertainty of the extrapolation from larger to smaller impact parameters. The agreement between data and simulation of p_T (ℓ) distribution indicate that additional uncertainties on the extrapolation from higher to lower p_T (ℓ) are not required. The uncertainty on the total prediction is less than 5% as this background is sub-dominant. The recoil resolution uncertainty is derived from data by $Z \to \mu\mu$ events. The uncertainty could affect the DY+jets estimation, which takes the $M_{\tau\tau}$ cut efficiency from simulation. The effect on the total predicted background is found to be negligible.
- The background prediction for the non-prompt background has a 30% uncertainty which is derived from a closure test of the method used in measuring its rate, performed over simulated samples. The impact on the prediction typically ranges between 5-25%.
- The uncertainty on the VV background estimate is 50%, which was checked in a dedicated validation region with enriched WW events in a similar topology to signal events. It was confirmed that agreement within the given uncertainty was observed.
- A conservative 100% uncertainty is assigned to the rare backgrounds (dominated by tW events).
- Uncertainties on data-simulation scale factors (SF) for b-tagging, trigger, lepton ID and isolation are between 1-6%.
- The propagated jet energy correction (JEC) uncertainty leads to typically less than 5% uncertainty on the overall prediction of the SM event yields.

Table 4: Typical relative uncertainties on the yields estimated with the background prediction methods in the signal region for each individual systematic uncertainty source.

Systematic uncertainty source	typical uncertainty
$t\bar{t}$ and DY+jets stat. unc. from MC	5-20%
$t\bar{t}$ modeling	$\lesssim 5$ %
"Tight to loose ratio" closure in MC	5-25%
DY+jets closure in data	$\lesssim 5$ %
VV cross section	5-10%
tW cross section	5-10 %
Lepton/Trigger/b-tag SF	1-6 %
Jet energy scale	1-5 %

7 Results

The predicted yields of the SM background processes in the SR are presented in Figures 3 and 4, compared to data corresponding to 10.1 fb^{-1} (low E_T^{miss} range) and 12.9 fb^{-1} (high E_T^{miss} range) of integrated luminosity, respectively. The predicted yields are determined using data assisted methods described in Section 5 and are summarized in Tables 5 and 6. The total uncertainty on

the yield for each SM process is composed of the systematic and statistic uncertainties described in Section 6.

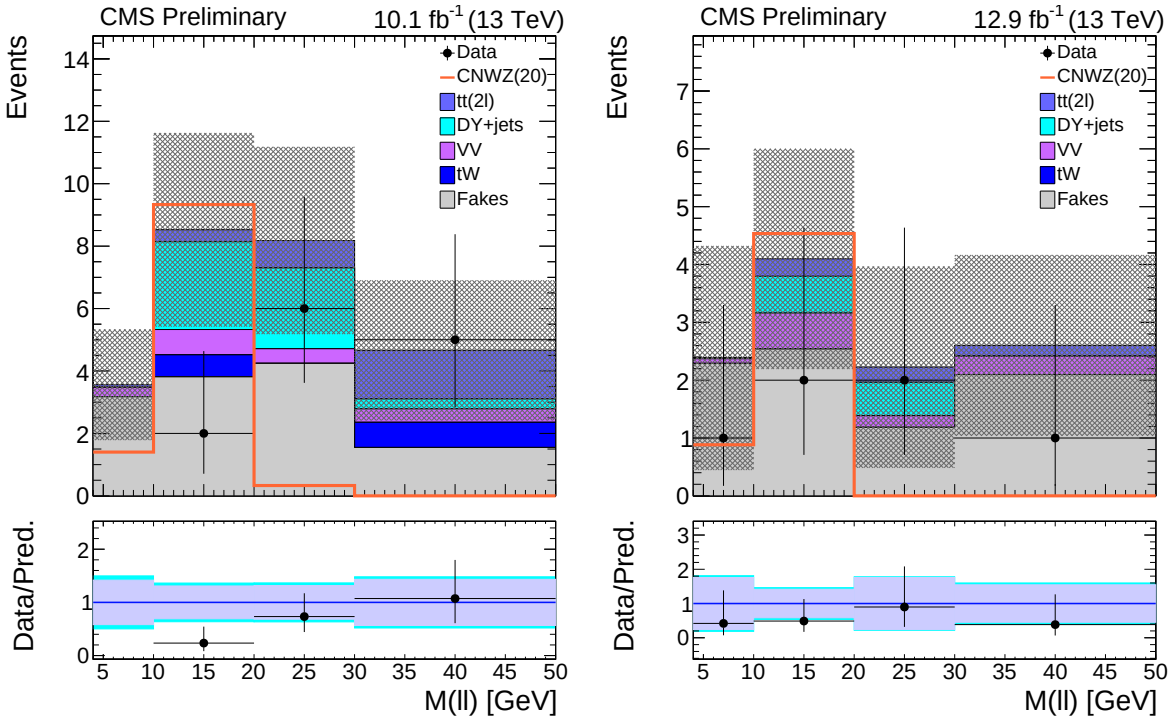

Figure 3: Dilepton mass distributions in data, compared with the SM predictions, in electroweakino-like signal region for two $E_{\mathrm{T}}^{\mathrm{miss}}$ ranges: $125 < E_{\mathrm{T}}^{\mathrm{miss}} < 200$ GeV (muon channel) (left) and $E_{\mathrm{T}}^{\mathrm{miss}} > 200$ GeV (muon and electron channels) (right) for 10.1 fb^{-1} and 12.9 fb^{-1} of integrated luminosity, respectively. The shaded grey band in the SM prediction is the total uncertainty, calculated from the statistical uncertainties in the data application regions and the systematic uncertainty for each SM background yield. In the ratio plot the light purple band indicates the statistical uncertainty, while the light cyan band includes both statistical and systematic uncertainties. The signal corresponding to $\tilde{\chi}_2^0\tilde{\chi}_1^{\pm} \to \tilde{\chi}_1^0\tilde{\chi}_1^0 Z W^*$ for a $\tilde{\chi}_2^0$ mass of 100 GeV and a difference (Δm) between $\tilde{\chi}_2^0$ and $\tilde{\chi}_1^0$ of 20 GeV is superimposed.

8 Interpretation

The results are interpreted in terms of $\tilde{\chi}_2^0\tilde{\chi}_1^{\pm} \to \tilde{\chi}_1^0\tilde{\chi}_1^0 Z^* W^*$ simplified model and of compressed $\tilde{\mathrm{t}}$ four body decay simplified models introduced in Section 2. As the signal yields come directly from simulation, additional systematic uncertainties are applied. We split these systematic uncertainties in two categories. One is the systematic uncertainty on the inclusive NLO+NLL [35, 36] cross section used for the normalization: it consists of varying the renormalization and factorization scale and parton distribution functions. The other category is the uncertainty on the acceptance times efficiency ($a \times \epsilon$) of the signal. To account for the renormalization and factorization scale uncertainties a 3% uncertainty is applied. Given the phase space covered by this analysis, the modeling of ISR that leads to the boost of the produced sparticle pair in the transverse plane is important. DY and $\mathrm{t\bar{t}}$ events were used to derive corrections of the ISR modeling from data of weakly and strongly produced processes. The results were compared to MADGRAPH v5 which is also used for the signal simulation. The electroweak production correction is applied to the $\tilde{\chi}_2^0\tilde{\chi}_1^{\pm}$ model and the strong production correction to

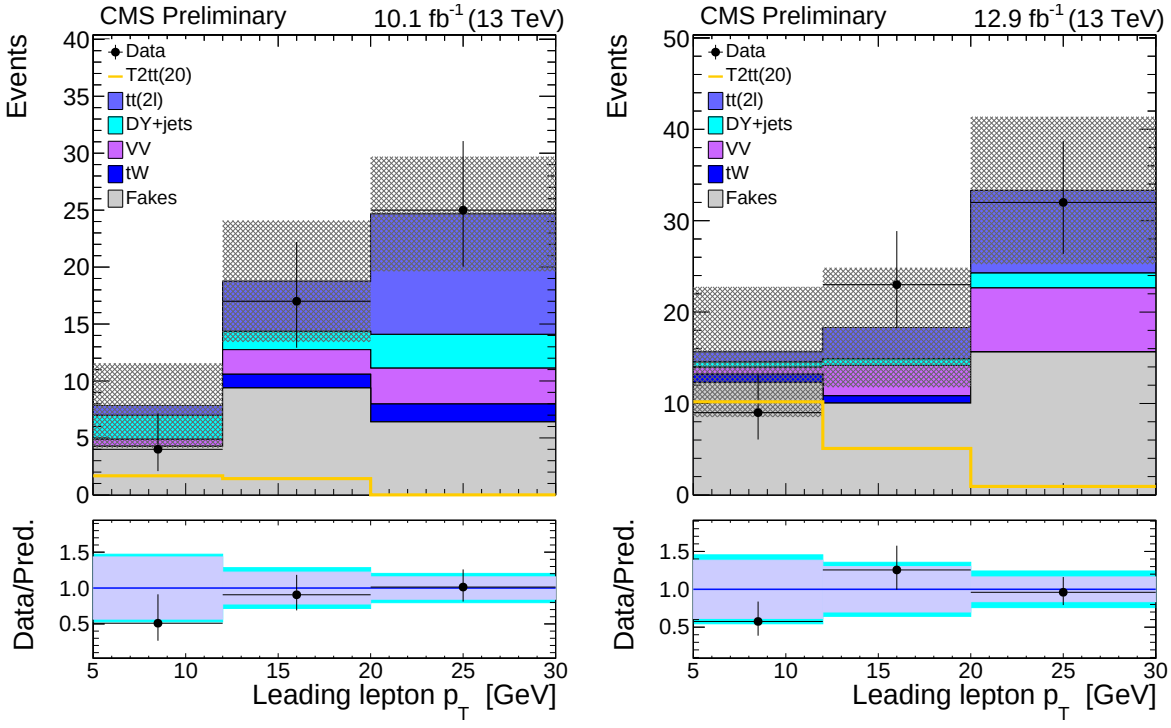

Figure 4: p_{T} distributions for the leading lepton in data, compared with the SM predictions, in $\widetilde{\mathrm{t}}$-like signal region for two $E_{\mathrm{T}}^{\mathrm{miss}}$ ranges: $125 < E_{\mathrm{T}}^{\mathrm{miss}} < 200$ GeV (muon channel) (left) and $E_{\mathrm{T}}^{\mathrm{miss}} > 200$ GeV (muon and electron channels) (right) for 10.1 fb^{-1} and 12.9 fb^{-1} of integrated luminosity, respectively. The shaded grey band in the SM prediction is the total uncertainty, calculated from the statistical uncertainties in the data application regions and the systematic uncertainty for each SM background yield. In the ratio plot the light purple band indicates the statistical uncertainty, while the light cyan band includes both statistical and systematic uncertainties. The signal corresponds to the model of $\widetilde{\mathrm{t}}$ pair production described in the text, where the $\widetilde{\mathrm{t}}$ mass is 350 GeV and $\Delta\mathrm{m}(\widetilde{\mathrm{t}}, \widetilde{\chi}_1^0)$ is 20 GeV.

Table 5: Predicted and data yields for electroweakino-like SR for 12.9 fb^{-1} and 10.1 fb^{-1} of integrated luminosity. Predicted yields and total uncertainties are reported.

Process	E_T^{miss} = [125-200]			
	$4 < M(\ell\ell) < 10$	$10 < M(\ell\ell) < 20$	$20 < M(\ell\ell) < 30$	$30 < M(\ell\ell) < 50$
$t\bar{t}(2\ell)$	0.1 ± 0.1	0.4 ± 0.2	0.9 ± 0.3	1.6 ± 0.5
DY	$0.0 + 0.05$	2.8 ± 1.4	2.6 ± 1.0	0.3 ± 0.2
VV	0.3 ± 0.2	0.8 ± 0.4	0.5 ± 0.2	0.4 ± 0.2
tW	$0.0 + 0.2$	0.7 ± 0.9	$0.0 + 0.2$	0.8 ± 1.0
Non-prompt leptons	3.2 ± 1.8	3.8 ± 2.6	4.2 ± 2.8	1.6 ± 2.0
Total SM prediction	3.6 ± 1.8	8.5 ± 3.1	8.2 ± 3.0	4.7 ± 2.3
Data	0	2	6	5

Process	E_T^{miss} = [200-inf]			
	$4 < M(\ell\ell) < 10$	$10 < M(\ell\ell) < 20$	$20 < M(\ell\ell) < 30$	$30 < M(\ell\ell) < 50$
$t\bar{t}(2\ell)$	$0.0 + 0.05$	0.3 ± 0.3	0.3 ± 0.2	0.2 ± 0.2
DY	$0.0 + 0.05$	0.6 ± 0.3	0.6 ± 0.4	$0.0 + 0.05$
VV	0.1 ± 0.1	0.6 ± 0.4	0.2 ± 0.1	0.3 ± 0.2
Non-prompt leptons	2.3 ± 1.9	2.5 ± 1.9	1.2 ± 1.7	2.1 ± 1.5
Total SM prediction	2.4 ± 2.1	4.1 ± 2.0	2.2 ± 1.8	2.6 ± 1.6
Data	1	2	2	1

Table 6: Predicted and data yields for $\widetilde{t}$-like SR for 12.9 fb^{-1} and 10.1 fb^{-1} of integrated luminosity. Predicted yields and total uncertainties are reported.

Process	E_T^{miss} = [125-200]		
	$5 < p_T(\ell_1) < 12$	$12 < p_T(\ell_1) < 20$	$20 < p_T(\ell_1) < 30$
$t\bar{t}(2\ell)$	0.9 ± 0.5	4.4 ± 0.9	10.6 ± 1.7
DY	2.1 ± 1.3	1.6 ± 0.7	3.0 ± 1.1
VV	0.6 ± 0.4	2.2 ± 1.1	3.2 ± 1.6
tW	0.0 ± 0.2	1.2 ± 1.4	1.6 ± 1.8
Non-prompt leptons	4.3 ± 3.5	9.4 ± 4.9	6.4 ± 4.0
Total SM prediction	7.9 ± 3.7	18.8 ± 5.3	14.7 ± 5.1
Data	4	17	25

Process	E_T^{miss} = [200-inf]		
	$5 < p_T(\ell_1) < 12$	$12 < p_T(\ell_1) < 20$	$20 < p_T(\ell_1) < 30$
$t\bar{t}(2\ell)$	1.1 ± 0.5	3.4 ± 0.9	9.1 ± 1.7
DY	0.6 ± 0.4	0.7 ± 0.4	1.6 ± 0.6
VV	0.7 ± 0.4	3.3 ± 1.7	7.0 ± 3.6
tW	0.9 ± 1.3	0.8 ± 1.1	0.0 ± 0.2
Non-prompt leptons	12.3 ± 7.0	10.0 ± 6.2	15.6 ± 7.0
Total SM prediction	15.6 ± 7.1	18.3 ± 6.6	33.3 ± 8.1
Data	9	23	32

the $\tilde{t}$ scan. We assign an uncertainty on these corrections to account for the fact that the processes used are only similar to the sparticle production. The uncertainties range from 10-20%. The uncertainty on the integrated luminosity is 6.2%. Uncertainty on the pileup is computed by varying the minimum-bias cross section by $\pm$ 5% and reweighting the pileup distribution accordingly. The systematic uncertainty on this source has been estimated to be within 1%. Leptons and b-tagging related efficiency for fast simulation are also derived and scale factors between fast and full simulation have been applied to the signal, together with a dedicated set of JEC corrections for fast simulation. The uncertainties related to these corrections lead to an average 5% uncertainty on the signal.
For the interpretation we use a binned likelihood approach, which includes the signal, Drell-Yan and $t\bar{t}$ control region bins in order to automatically account for signal in control regions. The uncertainties are added as log normal nuisance parameters and the DY+jets and $t\bar{t}$ background normalization are left free to float in the likelihood.
We derive at 95% confidence level (CL) the upper limits on the cross section. We use asymptotic results for the test statistic [37] and the CL_s criterion, that is described in [38, 39]. More details can be found in [40]. The interpretations are shown in Figure 5. For the electroweakino model we exclude $\tilde{\chi}_2^0$ masses of up to 195 GeV for a $\Delta m(\tilde{\chi}_2^0, \tilde{\chi}_1^0)$ of 20 GeV. This result slightly exceeds the expected exclusion, having observed less events in the electroweakino signal regions than expected.
Although the analysis is carried out for the $\tilde{\chi}_2^0\tilde{\chi}_1^\pm$ production in the Wino case, the sensitivity for higgsino case is our interest, where the mass difference between $\tilde{\chi}_2^0$ and $\tilde{\chi}_1^0$ are expected to be small as described in Section 1. In the higgsino case:
(i) It is pointed out in Ref. [9] that the $\tilde{\chi}_2^0 \to \tilde{\chi}_1^0 Z^*$ decay is a main source for OS dilepton as $\tilde{\chi}_1^\pm$ is closer in mass to $\tilde{\chi}_2^0$ than $\tilde{\chi}_1^0$.
(ii) The sum of the cross sections for pure higgsino $\tilde{\chi}_2^0\tilde{\chi}_1^0$ and $\tilde{\chi}_2^0\tilde{\chi}_1^\pm$ production is rougly a third of the cross section for $\tilde{\chi}_2^0\tilde{\chi}_1^\pm$ production in the Wino case. It should be noted that a $\tilde{\chi}_1^+\tilde{\chi}_1^-$ production in higgsino case is ignored, providing a conservative estimate.
This high branching fraction ($\tilde{\chi}_2^0 \to \tilde{\chi}_1^0 Z^*$) and the sum of the cross sections ($\tilde{\chi}_2^0\tilde{\chi}_1^0 + \tilde{\chi}_2^0\tilde{\chi}_1^\pm$) leads to an approximate factor of one third to the benchmark (Wino) cross section. Applying this factor to the excluded cross section in the benchmark scenario, it is found that the present analysis has sensitivity to a compressed higgsino scenario ($\Delta m < 20$ GeV) at approximately 100 GeV of the $\tilde{\chi}_2^0$ mass for the first time at the LHC.
For the $\tilde{t}$ four body decay we exclude, within the simplified model, $\tilde{t}$ masses up to 360 GeV for a $\Delta m(\tilde{t}, \tilde{\chi}_1^0)$ of 30 GeV.

9 Summary

A search for new physics in events with two soft opposite-sign leptons and missing transverse energy is presented using the data collected at 13 TeV in 2016 corresponding to an integrated luminosity of up to 12.9 fb^{-1}. The data is consistent with the standard model expectations. The results are interpreted in the framework of supersymmetric simplified models targeting electroweakino mass-degenerate spectra and in terms of $\tilde{t}$-$\tilde{\chi}_1^0$ mass-degenerate benchmarks. For the first time since LEP experiments a search probes the $\tilde{\chi}_2^0\tilde{\chi}_1^\pm \to \tilde{\chi}_1^0\tilde{\chi}_1^0 Z^* W^*$ process for mass differences (Δm) between $\tilde{\chi}_2^0$ and $\tilde{\chi}_1^0$ of less than 20 GeV. Assuming Wino production cross sections, $\tilde{\chi}_2^0$ masses up to 195 GeV are excluded for Δm of 20 GeV. For the $\tilde{t}$ four body decay, $\tilde{t}$ masses of up to 360 GeV is excluded for a $\Delta m(\tilde{t}, \tilde{\chi}_1^0) = 30$ GeV within the simplified model.

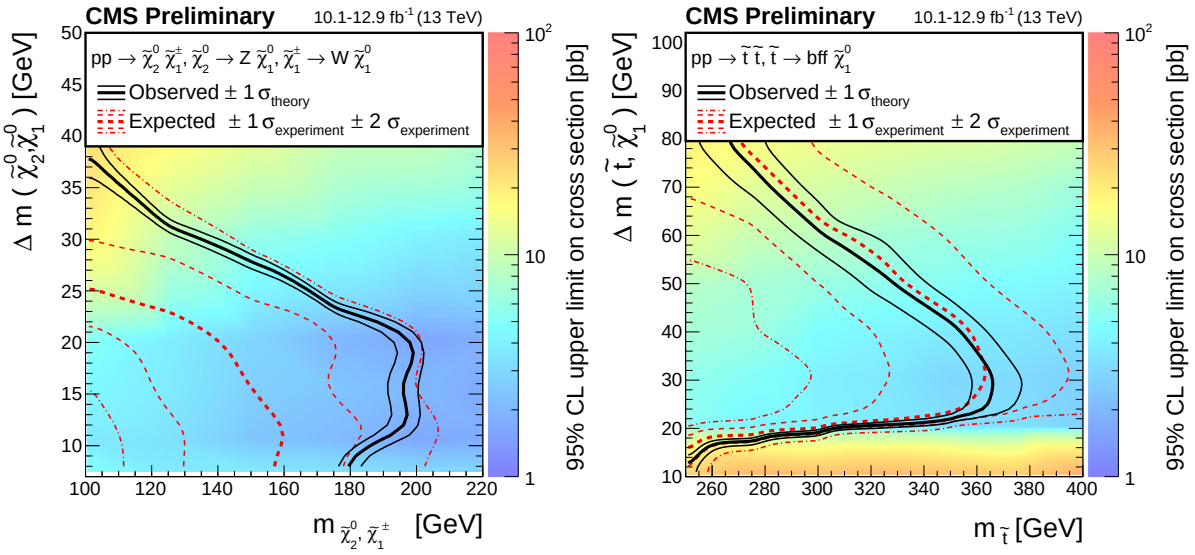

Figure 5: The observed exclusion contours (black curves) assuming the NLO+NLL cross sections, with the corresponding 1 standard deviation uncertainties for electroweak (left) and $\tilde{t}$ (right) searches. The dashed (red) curves present the expected limits with 1 and 2 standard deviation experimental uncertainties. Results are based on a simplified model of $\tilde{\chi}_2^0\tilde{\chi}_1^\pm \rightarrow \tilde{\chi}_1^0\tilde{\chi}_1^0 Z^* W^*$ process with a pure Wino production cross section in the electroweak analysis, while a simplified model of the $\tilde{t}$ pair production, followed by the $\tilde{t} \rightarrow ffb\tilde{\chi}_1^0$ decay is used for the $\tilde{t}$ analysis. Data corresponds to an integrated luminosity ranging from 10.1 fb^{-1} to 12.9 fb^{-1}.

References

[1] S. Dimopoulos and H. Georgi, "Softly broken supersymmetry and SU(5)", *Nucl. Phys. B* **193** (1981) 150, doi:10.1016/0550-3213(81)90522-8.

[2] E. Witten, "Dynamical breaking of supersymmetry", *Nucl. Phys. B* **188** (1981) 513, doi:10.1016/0550-3213(81)90006-7.

[3] M. Dine, W. Fischler, and M. Srednicki, "Supersymmetric technicolor", *Nucl. Phys. B* **189** (1981) 575, doi:10.1016/0550-3213(81)90582-4.

[4] S. Dimopoulos and S. Raby, "Supercolor", *Nucl. Phys. B* **192** (1981) 353, doi:10.1016/0550-3213(81)90430-2.

[5] N. Sakai, "Naturalness in supersymmetric GUTS", *Z. Phys. C* **11** (1981) 153, doi:10.1007/BF01573998.

[6] R. K. Kaul and P. Majumdar, "Cancellation of quadratically divergent mass corrections in globally supersymmetric spontaneously broken gauge theories", *Nucl. Phys. B* **199** (1982) 36, doi:10.1016/0550-3213(82)90565-X.

[7] G. F. Giudice, T. Han, K. Wang, and L.-T. Wang, "Nearly degenerate gauginos and dark matter at the LHC", *Phys. Rev. C* **81** (2010) 115011, doi:10.1103/PhysRevD.81.115011, arXiv:1004.4902.

[8] H. Baer, A. Mustafayev, and X. Tata, "Monojet plus soft dilepton signal from light higgsino pair production at LHC14", *Phys. Rev. D* **90** (2014) 115007, doi:10.1103/PhysRevD.90.115007, arXiv:1409.7058.

[9] Z. Han, G. D. Kribs, A. Martin, and A. Menon, "Hunting quasidegenerate Higgsinos", *Phys. Rev. D* **89** (2014) 075007, doi:10.1103/PhysRevD.89.075007, arXiv:1401.1235.

[10] ALEPH Collaboration, "Search for charginos nearly mass degenerate with the lightest neutralino in e+ e- collisions at center-of-mass energies up to 209 GeV", *Phys. Lett. B* **533** (2002) 223, doi:10.1016/S0370-2693(02)01584-8, arXiv:hep-ex/0203020.

[11] DELPHI Collaboration, "Searches for supersymmetric particles in e+ e- collisions up to 208 GeV and interpretation of the results within the MSSM", *Eur. Phys. J. C* **31** (2003) 421, doi:10.1140/epjc/s2003-01355-5, arXiv:hep-ex/0311019.

[12] L3 Collaboration, "Searches for scalar quarks in e^+e^- interactions at $\sqrt{s}$ = 189 GeV", *Phys. Lett. B* **471** (1999) 308, doi:10.1016/S0370-2693(99)01363-5, arXiv:hep-ex/9910020.

[13] C. Balázs, M. Carena, and C. E. M. Wagner, "Dark matter, light stops and electroweak baryogenesis", *Phys. Rev. D* **70** (2004) 015007, doi:10.1103/PhysRevD.70.015007, arXiv:hep-ph/0403224.

[14] CMS Collaboration, "Search for supersymmetry in events with soft leptons, low jet multiplicity, and missing transverse energy in protonproton collisions at $\sqrt{s}$ = 8 TeV", *Phys. Lett. B* **759** (2016) 9, doi:10.1016/j.physletb.2016.05.033, arXiv:1512.08002.

[15] J. Alwall et al., "MadGraph5: going beyond", *JHEP* **06** (2011) 128, doi:10.1007/JHEP06(2011)128, arXiv:1106.0522.

[16] NNPDF Collaboration, "Parton distributions for the LHC Run II", *JHEP* **04** (2015) 040, doi:10.1007/JHEP04(2015)040, arXiv:1410.8849.

[17] J. Alwall et al., "The automated computation of tree-level and next-to-leading order differential cross sections, and their matching to parton shower simulations", *JHEP* **07** (2014) 079, doi:10.1007/JHEP07(2014)079, arXiv:1405.0301.

[18] P. Nason, "A new method for combining NLO QCD with shower Monte Carlo algorithms", *JHEP* **11** (2004) 040, doi:10.1088/1126-6708/2004/11/040, arXiv:hep-ph/0409146.

[19] S. Frixione, P. Nason, and C. Oleari, "Matching NLO QCD computations with parton shower simulations: the POWHEG method", *JHEP* **11** (2007) 070, doi:10.1088/1126-6708/2007/11/070, arXiv:0709.2092.

[20] S. Alioli, P. Nason, C. Oleari, and E. Re, "A general framework for implementing NLO calculations in shower Monte Carlo programs: the POWHEG BOX", *JHEP* **06** (2010) 043, doi:10.1007/JHEP06(2010)043, arXiv:1002.2581.

[21] S. Alioli, P. Nason, C. Oleari, and E. Re, "NLO single-top production matched with shower in POWHEG: s- and t-channel contributions", *JHEP* **09** (2009) 111, doi:10.1007/JHEP02(2010)011, 10.1088/1126-6708/2009/09/111, arXiv:0907.4076. [Erratum: JHEP **02** (2010) 011].

[22] E. Re, "Single-top Wt-channel production matched with parton showers using the POWHEG method", *Eur. Phys. J. C* **71** (2011) 1547, doi:10.1140/epjc/s10052-011-1547-z, arXiv:1009.2450.

[23] T. Sjöstrand et al., "An Introduction to PYTHIA 8.2", *Comput. Phys. Commun.* **191** (2015) 159, doi:10.1016/j.cpc.2015.01.024, arXiv:1410.3012.

[24] S. Agostinelli et al., "GEANT4 — a simulation toolkit", *Nucl. Instr. and Meth. A* **506** (2003) 250, doi:10.1016/S0168-9002(03)01368-8.

[25] CMS Collaboration, "The Fast Simulation of the CMS Detector at LHC", Technical Report 3, CERN, 2011.

[26] R. Gröber, M. M. Mühlleitner, E. Popenda, and A. Wlotzka, "Light Stop Decays: Implications for LHC Searches", *Eur. Phys. J. C* **75** (2015) 420, doi:10.1140/epjc/s10052-015-3626-z, arXiv:1408.4662.

[27] CMS Collaboration, "Particle-flow event reconstruction in CMS and performance for jets, taus, and $E_{\mathrm{T}}^{\mathrm{miss}}$", CMS Physics Analysis Summary CMS-PAS-PFT-09-001, CERN, 2009.

[28] CMS Collaboration, "Performance of CMS muon reconstruction in pp collision events at $\sqrt{s} = 7$ TeV", *JINST* **7** (2012) P10002, doi:10.1088/1748-0221/7/10/P10002, arXiv:1206.4071.

[29] CMS Collaboration, "Studies of Higgs boson production in the four-lepton final state at $\sqrt{s} = 13$ TeV", CMS Physics Analysis Summary CMS-PAS-HIG-15-004, CERN, 2016.

[30] M. Cacciari, G. P. Salam, and G. Soyez, "The Anti-k(t) jet clustering algorithm", *JHEP* **04** (2008) 063, doi:10.1088/1126-6708/2008/04/063, arXiv:0802.1189.

[31] CMS Collaboration, "Identification of b quark jets at the CMS Experiment in the LHC Run 2", CMS Physics Analysis Summary CMS-PAS-BTV-15-001, CERN, 2016.

[32] CMS Collaboration, "Search for new physics with same-sign isolated dilepton events with jets and missing transverse energy at the LHC", *JHEP* **06** (2011) 077, doi:10.1007/JHEP06(2011)077, arXiv:1104.3168.

[33] ATLAS Collaboration, "Measurement of spin correlation in top-antitop quark events and search for top squark pair production in pp collisions at $\sqrt{s} = 8$ TeV using the ATLAS detector", *Phys. Rev. Lett.* **114** (2015) 142001, doi:10.1103/PhysRevLett.114.142001, arXiv:1412.4742.

[34] CMS Collaboration, "Measurements of $\mathrm{t\bar{t}}$ spin correlations and top quark polarization using dilepton final states in pp collisions at $\sqrt{s} = 8$ TeV", *Phys. Rev. D* **93** (2016) 052007, doi:10.1103/PhysRevD.93.052007, arXiv:1601.01107.

[35] B. Fuks, M. Klasen, D. R. Lamprea, and M. Rothering, "Gaugino production in proton-proton collisions at a center-of-mass energy of 8 TeV", *JHEP* **10** (2012) 081, doi:10.1007/JHEP10(2012)081, arXiv:1207.2159.

[36] B. Fuks, M. Klasen, D. R. Lamprea, and M. Rothering, "Precision predictions for electroweak superpartner production at hadron colliders with Resummino", *Eur. Phys. J. C* **73** (2013) 2480, doi:10.1140/epjc/s10052-013-2480-0, arXiv:1304.0790.

[37] G. Cowan, K. Cranmer, E. Gross, and O. Vitells, "Asymptotic formulae for likelihood-based tests of new physics", *Eur. Phys. J. C* **71** (2011) 1554, doi:10.1140/epjc/s10052-011-1554-0, 10.1140/epjc/s10052-013-2501-z, arXiv:1007.1727. [Erratum: Eur. Phys. J.C73,2501(2013)].

[38] T. Junk, "Confidence level computation for combining searches with small statistics", *Nucl. Instr. and Meth. A* **434** (1999) 435, doi:10.1016/S0168-9002(99)00498-2, arXiv:hep-ex/9902006.

[39] A. L. Read, "Presentation of search results: the CL_s technique", *J. Phys. G* **28** (2002) 2693, doi:10.1088/0954-3899/28/10/313.

[40] ATLAS and CMS Collaborations, "Procedure for the LHC Higgs boson search combination in Summer 2011", CMS-NOTE-2011-005, ATL-PHYS-PUB-2011-11, CERN, 2011.